Heliyon 7 (2021) e06387

Contents lists available at ScienceDirect

Heliyon

journal homepage: www.cell.com/heliyon

Research article

The study of antiviral drugs targeting SARS-CoV-2 nucleocapsid and spike proteins through large-scale compound repurposing

Xuqiao Hu [a,b,1], Zhenru Zhou [a,1], Fei Li [c], Yang Xiao [c], Zhaoyang Wang [a], Jinfeng Xu [a,*], Fajin Dong [a,**], Hairong Zheng [c,***], Rongmin Yu [b,d,e,****]

[a] Department of Ultrasound, First Affiliated Hospital of Southern University of Science and Technology, Second Clinical Medical College of Jinan University (Shenzhen People's Hospital), Shenzhen, 518020, China
[b] Integrated Chinese and Western Medicine Postdoctoral Research Station, Jinan University, Guangzhou, 510632, China
[c] Paul C. Lauterbur Research Center for Biomedical Imaging, Institute of Biomedical and Health Engineering, Shenzhen Institutes of Advanced Technology, Chinese Academy of Sciences, 1068 Xueyuan Avenue, SZ University Town, Shenzhen, 518055, China
[d] Department of Pharmacology, College of Pharmacy, Jinan University, 601 Huangpu Avenue West, Guangzhou, 510632, China
[e] Biotechnological Institute of Chinese Materia Medica, Jinan University, 601 Huangpu Avenue West, Guangzhou, 510632, China

ARTICLE INFO

Keywords:
SARS-CoV-2
Drug screen and repurposing
Small molecule microarray chip
Antiviral compounds

ABSTRACT

Contributing to severe acute respiratory syndrome coronavirus 2 (SARS-CoV-2) clinical treatment, a drug library encompassing approximately 3,142 clinical-stage or FDA-approved small molecules is profiled to identify the candidate therapeutic inhibitors targeting nucleocapsid protein (N) and spike protein (S) of SARS-CoV-2.

16 screened candidates with higher binding affinity are evaluated via virtual screening. Comparing to those under trial/temporarily used antivirus drugs (i.e., umifenovir, lopinavir), ceftriaxone, cefotaxime, and cefuroxime show higher binding affinities to the N-terminal domain of N protein (N-NTD), C-terminal domain of N protein (N-CTD), and receptor-binding domain of S protein (S-RBD). Cefotaxime and cefuroxime have high binding affinities towards S-RBD with angiotensin-converting enzyme 2 (ACE2) complex via influence the critical interface sites at the interface of S-RBD (Arg^{403}, Tyr^{453}, Trp^{495}, Gly^{496}, Phe^{497}, $Asn^{501}$and Tyr^{505}) and ACE2 (Asn^{33}, His^{34}, Glu^{37}, Asp^{38}, Lys^{353}, Ala^{386}, Ala^{387}, Gln^{388}, Pro^{389}, Phe^{390} and Arg^{393}) complex.

1. Introduction

Severe acute respiratory syndrome coronavirus 2 (SARS-CoV-2) has been identified as the causative agent for the coronavirus disease 2019 (COVID-19) [1, 2, 3]. The COVID-19 has rapidly spread to more than 220 countries and causes over 103 million cases and 2.2 million deaths until 4th February 2021 (https://covid19.who.int/). Indeed, an effective medical method is in great demand.

Genomic sequencing suggests that the pathogenic coronavirus shares 79.5–96.2% sequence identity to a bat coronavirus [4]. SARS-CoV-2 coronaviruses are enveloped, positive-sense, single-stranded RNA viruses with 10 open reading frames in the genome (Figure 1A). The RNAs encode four main structural proteins (envelop (E), membrane (M), spike (S), and nucleocapsid (N) proteins) and other accessory proteins (Figure 1B) [5, 6]. The S protein of SARS-CoV-2 (Figure 1C-E) contains a receptor-binding domain (S-RBD) (Protein Data Bank (PDB) ID: 7BWJ), which interacts with angiotensin-converting enzyme 2 (ACE2) in host cells and mediates receptor recognition/membrane fusion [7, 8]. As shown in Figure 1F, N protein of SARS-CoV-2 (PDB ID: 6VYO and 6WZQ) is reported to be a multifunctional RNA binding protein, which is necessary for viral RNA transcription and replication, modulating the metabolism of host cells [9]. The multifunctional properties of S and N proteins make them promising targets in battling SARS-CoV-2 by interfering with viral cellular invasion or replication [9, 10, 11, 12].

Even though the structural information of N-NTD, N-CTD and S-RBD, are well-reported [13, 14], the development of novel drugs is still

* Corresponding author.
** Corresponding author.
*** Corresponding author.
**** Corresponding author.
E-mail addresses: xujinfeng@yahoo.com (J. Xu), dongfajin@szhospital.com (F. Dong), hr.zheng@siat.ac.cn (H. Zheng), tyrm@jnu.edu.cn (R. Yu).
[1] These authors contributed equally: Xuqiao Hu, Zhenru Zhou.

https://doi.org/10.1016/j.heliyon.2021.e06387
Received 29 December 2020; Received in revised form 9 February 2021; Accepted 24 February 2021

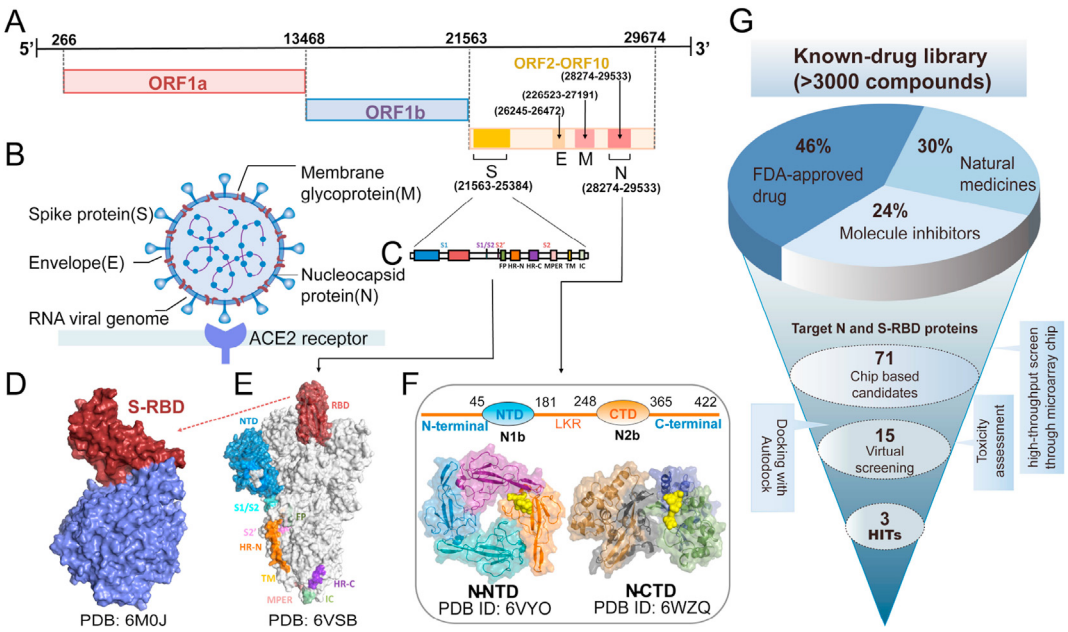

Figure 1. Analysis of the genome, structure, and target protein of SARS-CoV-2. (A) A genomic organization with structural domains. (B) The structure of SARS-CoV-2. (C) Domain structure of the SARS-CoV spike protein. NTD: N-terminal domain, RBD: receptor-binding domain, S1/S2: S1/S2 protease cleavage site, S2': S2′ protease cleavage site, FP: fusion peptide, HR-N, and HR-C: heptad repeat regions N and C, TPER: membrane-proximal outer region, TM: transmembrane domain, IC: cytoplasmic tail. Arrows denote protease cleavage sites. (D) Crystal structure of the RBD (cyan) in a complex of the human receptor ACE2 (green). (E) The crystal structure of the SARS-CoV-2 spike protein. (F) Domain architectures of SARS-CoV-2 nucleocapsid protein. NTD: N-terminal RNA binding domain; CTD: C-terminal dimerization domain. LKR: serine/arginine-rich linker domain. The crystal structure SARS-CoV-2 N protein includes the RNA binding domain (NTD) and the N2b domain (CTD). (G) High-throughput screening workflow to identify inhibitors that target SARS-CoV-2 N and S-RBD proteins.

limited. Due to the urgent requirement of specific antiviral drugs, a number of broad-spectrum antiviral drugs currently being explored in clinical trials for the treatment of COVID-19, such as lopinavir, ritonavir and remdesivir [15]. Unfortunately, it was reported such drugs could only provide limited efficacy and even seem to have possible toxic side effects [16]. To control the SARS-CoV-2 disaster, it is critically important to discover the specific anti-SARS-CoV-2 drugs with enhanced efficiency and safety. Repurposing of known drugs is, therefore, becoming a promising alternative strategy for expanding potential COVID-19 medical treatment.

To identify existing drugs that could harbor antiviral activity against SARS-CoV-2, a high-throughput re-profiling screen using entity small molecule inhibitors microarray chips with a drug library of 3,142 were performed in this study (Figure 1G). The library includes FDA-approved medicines, traditional Chinese medicine monomers, and additional developing small molecule inhibitors. This library chip is suitable for pure/total protein-small molecule interactions [17, 18, 19, 20] and nucleic acid-small molecule interactions [21, 22]. Comparing to novel drug development, the known pharmacological and safety profiles would streamline the drug development, which subsequently benefits both preclinical and clinical evaluation of these drugs for potential therapeutics. Furthermore, the molecule interactions between chip-screened candidates and N and S-RBD protein receptors would also provide new insight into the pharmacology mechanism on SARS-CoV-2 treatment.

2. Results and discussion

2.1. Large-scale screens of the known-drug library in microarray chip

2.1.1. The development of a high-throughput screening analysis

A high-throughput assay for large-scale screening of known drugs targeting N and S-RBD protein is developed via this project. Purified spike receptor-binding domain (S-RBD, residues 319-543) and the full length of N protein (residues 1-419) were obtained from Ebiocore Ltd. (http://www.ebiocore.com/), and their purity is confirmed by Bicinchoninic Acid Protein Assay and Sodium Dodecyl Sulfate Polyacrylamide Gel Electrophoresis (SDS-PAGE). As indicated, the purity of N and S-RBD protein exceeds 90% and 97.6%, respectively, which meet the requirement of large-scale screening [3].

As shown in Figure S1F, a small molecule microarray consisting of 3,142 molecules is employed for the experiment [19]. Small molecules are fixed on the microarrays through isocyanate-coated glass slides according to the literature elsewhere [20, 23, 24]. The purified N and S-RBD proteins are then labeled with Cy5 via the incubation of Cy5-monofunctional reactive dye [21, 25, 26, 27]. Sensitivity and specificity are assessed by using a gradual content of Cy5 labeled proteins, where Cy5-BSA/BSA are used as positive/negative controls (Figure S1B). The positive Cy5-BSA and the negative BSA protein dots show bright and dark fluorescence, respectively. The intensity of the fluorescence for protein dots could be quantified via scanning (635 nm wavelength). Both N and S-RBD protein quantity are correlated with the fluorescent signal, where the minimum detection limit is 1.56 ng, indicating high feasibility and sensitivity (Figure S1A and B).

To assess the robustness and reproducibility of the optimized fluorescence-based assay in a high-throughput screening configuration, the molecule is printed in triplicate on the chip. Before the protein incubation, the auto-fluorescent intensity of the background (3,142 small molecules) is evaluated under a fluorescent scanner at 635 nm. As shown in Figure S1C, the correlation coefficient (R^2) of two printed microarray chips is calculated to be 0.96, which suggesting the consistency of the chips. N and S-RBD proteins are separately incubated in two different printed microarrays. Their fluorescence intensities are scanned (635 nm), and the fluorescent intensity of triplicate spots are then extracted according to the literature [19]. As depicted in Figure S3D and S3E, the correlation coefficients (R^2) of triplicated spots for N protein are 0.94, 0.91, and 0.94. As for S-RBD protein, they are calculated to be 0.95, 0.94, and 0.96. The average value of the signal to noise ratio (SNR) for the triplicated spots are used for further analysis.

2.1.2. The chip screening analysis for 3142 medical approved small molecules

N and S-RBD proteins separately interact with a microarray chip (Figure 2A). SNR and fold change scores (FC) are used to assess the potential inhibitors, where 72 potential positive molecules are identified (Table S2). Figure 2B and 2C provide the example which is randomly selected from the same positions of both experimental chip and the negative control chip. A total of 30 spots with the highest FC are selected for N and S-RBD proteins (15 for each), and the results are shown in Figure 2D and 2E. Interestingly, it is found that a considerable amount of candidates present a considerable high FC toward N and S-RBD proteins at the same time (Table S2).

Those clinically approved drugs have been previously optimized for safety and bioavailability. For example, bismuth subnitrate with an FC of 4.33 is a specific anti-*Helicobacter pylori* drug [28], and cefotaxime (FC = 1.86) is known as a broad-spectrum antibiotic [29]. The in *vitro* cytotoxicity assays of the drug candidates are measured by CCK8 assay on Vero cells. As shown in Figure S2, the cell survival rate is close to 100% at 0.3 μM, and even at a higher concentration of 20 μM, an over 80% rate is still maintained, demonstrating the safety of the drugs.

2.2. Structure-based drug screening

2.2.1. The binding energy analysis of top 16 active molecules from chip screening

To further identify the effective inhibitors of SARS-CoV-2 N and S-RBD receptors among those screened drugs, 16 active candidates are selected for further molecular docking analysis. As listed in Table S1, the well-elaborated crystal structures of the N-terminal domain (N-NTD, PDB: 6VYO), C-terminal domain (N-CTD, PDB: 6WZQ), and S-RBD (PDB:7BWJ) are utilized for docking. The high-throughput virtual screening of the candidates using the docking approach results in a broad range of binding affinity, typically ranging from -2.67 to-13.24 kcal/mol (Figure 3A). A series of antibiotics (cefotaxime, cefuroxime, ceftriaxone, ampicillin, cefamandole nafate, sulbactam sodium) and a multi-target inhibitor (KW2449) show considerable high binding affinities for both N protein and S-RBD, which is consistent with the FC results.

The data from Figure 3B suggest that ceftriaxone has the highest binding affinity toward both N-CTD (-13.24 kcal/mol) and N-NTD (-11.56 kcal/mol). As a typical third-generation cephalosporin against a broad spectrum of gram-negative bacteria, ceftriaxone has a significant bactericidal effect, for example, *Pneumococcus*, *Streptococcus*,

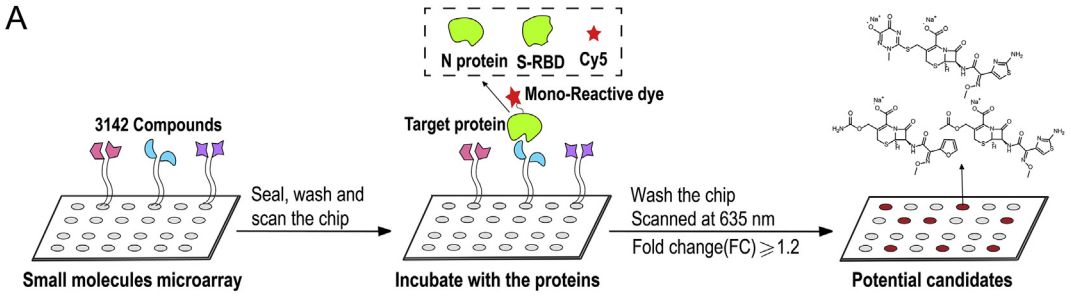

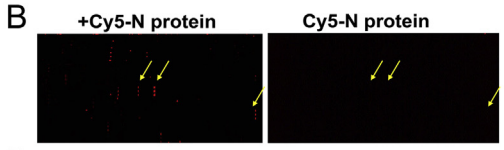

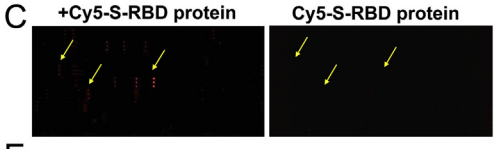

D

Name	+Cy5-N	-Cy5-N	SNR(+)	Ratio	*P*-value
Bismuth(III) Subnitrate			4.55	4.33	5.1×10^{-6}
Oxytocin			4.52	3.74	6.3×10^{-4}
1,2-Dilinoleoyl-3-oleoyl-rac-glycerol			2.29	2.20	2.3×10^{-2}
Glucagon			2.33	2.07	7.2×10^{-4}
Cefotaxime #			1.94	1.86	2.8×10^{-5}
Sulbactam			1.94	1.81	4.9×10^{-3}
Valproic Acid #			1.74	1.69	1.1×10^{-3}
Cefuroxime #			1.88	1.69	1.3×10^{-2}
Ceftriaxone # Hemiheptahydrate			1.91	1.66	3.1×10^{-5}
Ampicillin #			1.81	1.65	4.7×10^{-2}
Natamycin			1.93	1.64	2.5×10^{-4}
Cefamandole Nafate			1.79	1.62	3.5×10^{-3}
Cephalexin Monohydrate			1.74	1.61	3.2×10^{-3}
Sulbactam #			1.63	1.58	1.5×10^{-3}
Trifluridine			1.64	1.57	2.0×10^{-5}

Sodium salt

E

Name	+Cy5-S-RBD	-Cy5-S-RBD	SNR(+)	Ratio	*P*-value
Oxytocin			3.70	3.32	1.5×10^{-5}
KW 2449			2.09	1.76	3.9×10^{-4}
Cefuroxime #			1.76	1.65	5.2×10^{-4}
Bismuth(III) Subnitrate			1.78	1.64	7.1×10^{-4}
Sulbactam			1.78	1.60	2.0×10^{-3}
Cefotaxime #			1.63	1.55	4.2×10^{-4}
Dexrazoxane Hydrochloride			1.61	1.54	2.7×10^{-3}
7-Aminocephalosporanic acid			1.65	1.52	1.3×10^{-3}
Sulbactam #			1.56	1.47	6.2×10^{-4}
Cefixime			1.58	1.47	2.6×10^{-4}
Cefoperazone			1.59	1.47	3.4×10^{-4}
Trifluridine			1.69	1.46	3.2×10^{-2}
1,2-Dilinoleoyl-3-oleoyl-rac-glycerol			1.58	1.46	2.4×10^{-3}
Cefamandole Nafate			1.50	1.45	2.6×10^{-4}
Natamycin			1.86	1.44	3.6×10^{-3}

Sodium salt

Figure 2. Identification of small molecule inhibitors binding to SARS-CoV-2 full-length N protein and S-RBD protein by molecular chip technology. (A) Schematic of the binding procedure for detecting small molecule and protein based on small molecule microarray. (B) The positive compound that binds to Cy5-labeled N protein (*left*). A control experiment was carried out without N protein (*right*). The 71 candidates of N protein-interacting compounds were identified by comparing the signals from the two microarrays. (C) The positive compound that binds to Cy5-labeled S-RBD protein (*left*). A control experiment was carried out without S-RBD protein (*right*). The 71 candidates of S-RBD protein-interacting compounds were identified by comparing the signals from the two microarrays. (D) Representative the 15 protein spots with the largest fold change of N protein. (E) Representative the top 15 compounds for S-RBD protein-interacting. Scan the Cy5 signals at 635 nm +, in the presence of Cy5-S-RBD protein; −, in the presence of Cy5 alone.

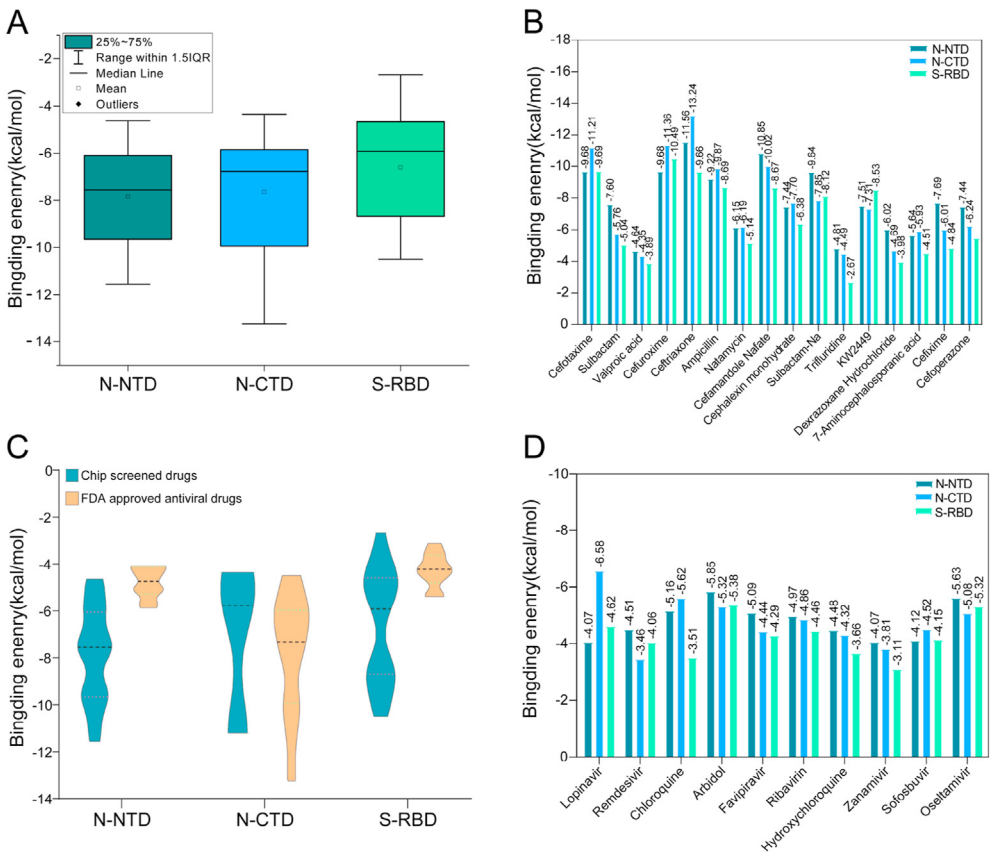

Figure 3. High-throughput screening of potential antiviral drugs for the N and S proteins of SARS-CoV-2. (A) The box plot shows the range of binding affinities (kcal/mol) for N-NTD (dark green), N-CTD (blue), and S-RBD (pale green) with the optimal mean values. (B) The bar graph shows the binding affinity (kcal/mol) of the selected docking drug to N-NTD, N-CTD and S-RBD, ranging from −2.67 to −13.24 kcal/mol. The high negative score indicates the maximum binding affinity. (C) The violin plot shows the range of binding affinities (kcal/mol) for chip screened drugs (teal) and FDA approved antiviral drugs (bright orange) for N-NTD, N-CTD, and S-RBD. (D) The bar chart shows the binding affinity scores in kilocalorie per mole for selected approved drugs.

Meningococcus, *Gonococcus,* and *Haemophilus influenza* [30]. Molecular docking results in Figure 3C also reveal ceftriaxone to have a considerable high binding affinity of -9.66 kcal/mol with S-RBD, which is slightly lower than other antibiotic drugs of cefuroxime (-10.49 kcal/mol) and cefotaxime (-9.69 kcal/mol).

This study also compares the relative binding affinities of those screened compounds with the antiviral drugs that are currently under clinical trials or temporarily used for SARS-CoV-2 (lopinavir, remdesivir, chloroquine, umifenovir, favipiravir, ribavirin, hydroxychloroquine, zanamivir, sofosbuvir, and oseltamivir). As shown in Figure 3C and 3D, compared to those drugs, screened candidates (i.e., ceftriaxone) show superior binding affinities. For example, lopinavir has a higher binding affinity toward N-CTD (-6.58 kcal/mol) amount those under trial/temporarily used drugs, but it still is comparatively less than the ceftriaxone (-13.24 kcal/mol) (Figure 3C-D). Similarly, even though umifenovir (Figure 3D) has shown high binding affinities toward both N-NTD (-5.85 kcal/mol) and S-RBD (-5.38 kcal/mol), the screened drug cefuroxime has better performance (N-NTD: -9.68 kcal/mol, S-RBD: -10.49 kcal/mol).

2.2.2. *Binding site analyses of screened drugs against N-NTD and N-CTD*

It is reported that the N protein is highly expressed during infection, which could induce a protective immune response against SARS-CoV-2 [31]. NTD and CTD domains play a pivotal role in N protein function, where the N-NTD interacts with viral RNA [32], while N-CTD is responsible for dimer formation in the RNA process [33]. These specific structural domains can be targeted with small molecules to disrupt the viral attachment and invade the host. Therefore, it is necessary to further study the small molecules targeting the NTD and CTD domains of N protein (Figure 4A).

From the post docking interaction analysis (Figure 4), ceftriaxone has shown the most favorable binding affinity toward A&D and A&B chains in tetrameric N-NTD and N-CTD, respectively. It is known that the N-NTD has a whole right-handed fold structure with an expanded ring in the middle, which is divided into palm and finger areas [13, 14]. One of the fingers called basic fin contains more basic amino acid residues, indicating the possible various combination models of N-NTD. As indicated in the "ceftriaxone-N-NTD complex", it is stabilized by five hydrogen bonds with the compounds through Asn^{153} and Thr^{148} in N-NTD (Figure 4B and 4C). As for the ceftriaxone-N-CTD complex (Figure 4F), three hydrogen bonds with Asp^{341}, Leu^{339}, and Arg^{259} of N-CTD are observed (Figure 3G). The specificity of ceftriaxone binding to N-NTD and N-CTD could be of potential interest for further validation and understanding of the mechanism.

Apart from ceftriaxone, cefuroxime also yields a high binding affinity of -11.36 kcal/mol toward N-CTD (Figure S3H, K), while cefamandole nafate seems to be the second-best toward N-NTD (next to ceftriaxone), which have a binding affinity of -10.85 kcal/mol (Figure S3B, E). Both cefuroxime and cefamandole nafate belong to the widely used cephalosporin class of antibiotics. Cephalosporins is the β-lactam antibiotics and are derivatives of 7-aminocephalosporanic acid (7-ACA) in β-lactam antibiotics. They have similar bactericidal mechanisms and are used for the treatment of respiratory tract infections among other indications [34]. The results in Figure S5B, E suggest that the cefuroxime and cefamandole nafate could bind within the nucleophilic residues of the N-NTD (Thr^{115}, Thr^{49} and Thr^{148}) and N-CTD (Thr^{334}, Thr^{332}) proteins via the conventional hydrogen/carbon-hydrogen bonds.

To further understand the screened drugs, the antiviral drugs that under clinical trial or temporarily used are also studied. The data from Figure 4D and E suggest that umifenovir prefers N-NTD with a binding affinity of -5.85 kcal/mol via conventional hydrogen bodings toward Leu^{159}, Leu^{161}, and Leu^{167} of D chain, and the rest of the key residues involved are from the D chain of carbon-hydrogen bond and sulfur-X in tetrameric N-NTD. As for N-CTD, the favorite drug is lopinavir, which has a conventional hydrogen bond with interacting with the Glu^{323} in the B chain of the N-CTD (Figure 4H, I). As illustrated in Figure S3, all the

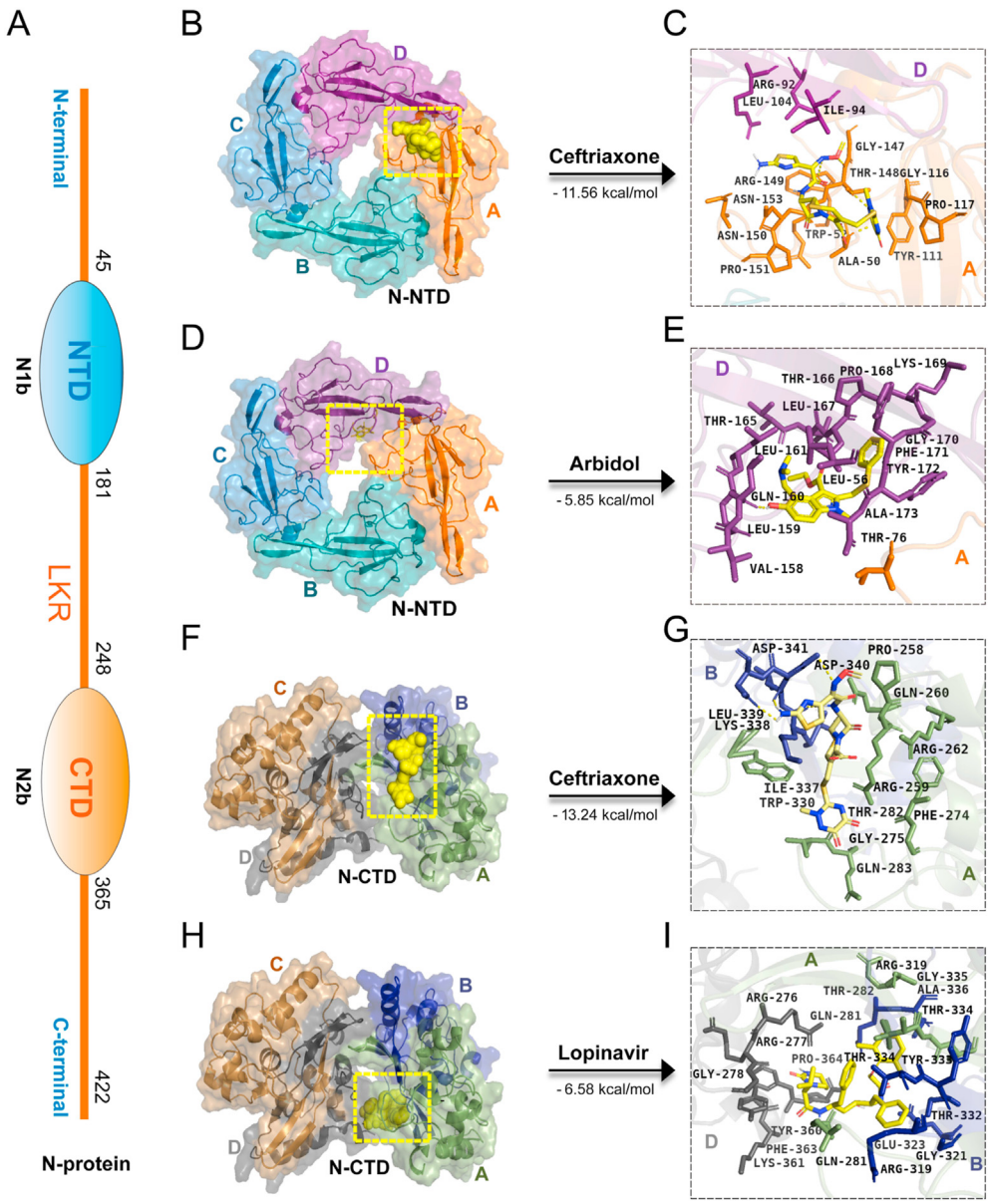

Figure 4. Antiviral drugs binding modes for N-NTD and N-CTD of N protein. (A) Schematic of N protein primary structure colored by the domain. NTD, N-terminal domain; CTD, C-terminal domain. (B and D) Ceftriaxone and umifenovir binding mode (yellow) to N-NTD protein (colors indicating chains). (C and E) Close-up view of ceftriaxone (yellow sticks) and umifenovir (yellow sticks) binding to the N-NTD protein chains (sticks). Yellow dotted lines indicate hydrogen bonds. (F and H) Ceftriaxone (yellow spheres) and lopinavir (yellow spheres) binding mode to N-CTD domains (colors indicating chains). (G and I) Close-up view of ceftriaxone (yellow sticks) and lopinavir (yellow sticks) binding to N-CTD (sticks). Yellow dotted lines indicate hydrogen bonds.

binding patterns mentioned above are vicinal to the active site pockets of N protein. The target receptor hydrogen binding and hydrophobic surfaces are summarized in Figure S3D-F and J-L.

2.2.3. Binding sites analyses of screened drugs against S-RBD

The RBD domain of S protein, which is mainly responsible for viral-host recognition (Figure 5A) [10], can be targeted with small molecules to disrupt or abolish the virus attachment to the host receptor ACE2. The interaction analysis of S-RBD (Figure 5A–C and S4) reveals that cefuroxime is more likely to bind to the region, where is vicinal to ACE2 binding sites that have β-sheet primary structure. For example, cefuroxime and cefotaxime have high binding affinities toward S-RBD protein with binding affinities of -10.49 and -9.69 kcal/mol, respectively. As shown in Figure 5C, conventional hydrogen bonds are found between cefuroxime and Ala^{352}, Asn^{354}, Ser^{349}, Asn^{448}, whereas cefotaxime firms conventional hydrogen bonds with Arg^{509}, Phe^{342}, Ala^{344}, Tyr^{451}, Asn^{448} and carbon-hydrogen bond with Leu^{441} (Figure S4).

Besides the screened drugs, umifenovir and S-RBD protein have the highest binding affinity (-5.38 kcal/mol) among those under clinical trial or temporarily used antiviral drugs. The data in Figure 5D suggest Asp^{428} form hydrogen bond interaction with the umifenovir along with two hydrophobic Pi-Alkyl bonds associated with Pro^{426} and Phe^{464}. It is also found that the screened drugs have relatively higher binding affinity than umifenovir in S-RBD protein, for example, ceftriaxone (-9.66 kcal/mol), ampicillin (-8.69 kcal/mol), and cefamandole nafate (-8.67 kcal/mol). This is likely due to the higher amount of critical residues involved in the binding, leading to more hydrogen bonds between protein and drugs.

As shown in Figure S5, all the interacted residues in the S-RBD protein are in the active site region. The target receptor hydrogen bonding and solvent accessible surfaces are depicted in Figure S4. The therapeutical description of screened drugs is also described in the supporting information (Table S3).

2.2.4. Occupying binding sites of S protein RBD-ACE2 complex upon interaction with cefuroxime and cefotaxime

It is known that the binding between S-RBD and ACE2 plays a key role in the recognition and infection of the virus to the host cell (Figure 6A) [10,35]. Therefore, the study of the RBD-ACE2 complex is important for drug evaluation. In this project, the docking of screened candidates with the complex structure is also conducted (Figure 6B). The atomic-level

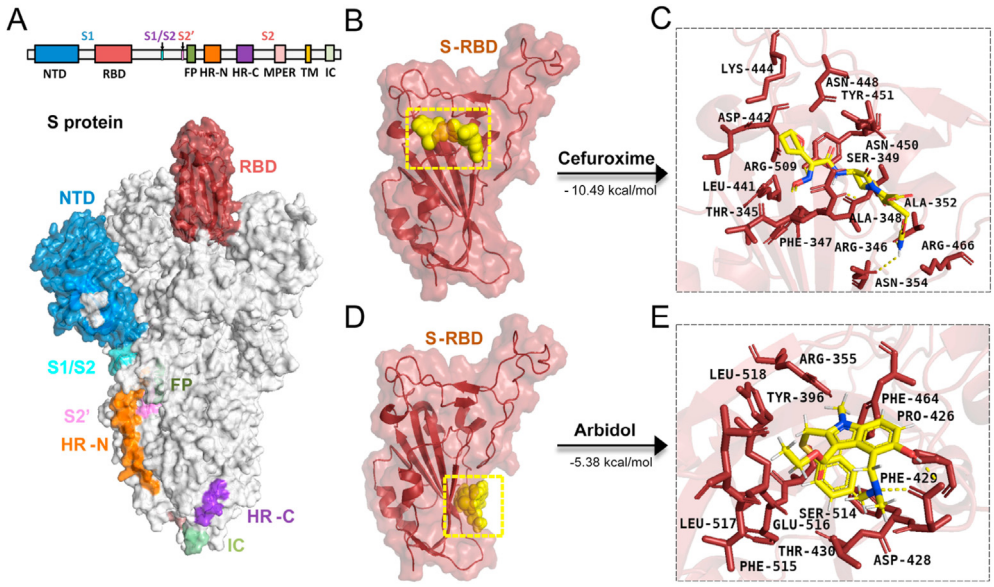

Figure 5. Screened drug-binding modes for RBD of Spike (S) protein. (A) Schematic of S protein primary structure colored by the domain. RBD, receptor-binding domain. (B and D) Cefuroxime (yellow spheres) and umifenovir (yellow spheres) binding mode to S-RBD protein. (C and E) Close-up view of Cefuroxime (yellow sticks) and umifenovir (yellow sticks) binding to the S-RBD protein chains (sticks). Yellow dotted lines indicate hydrogen bonds.

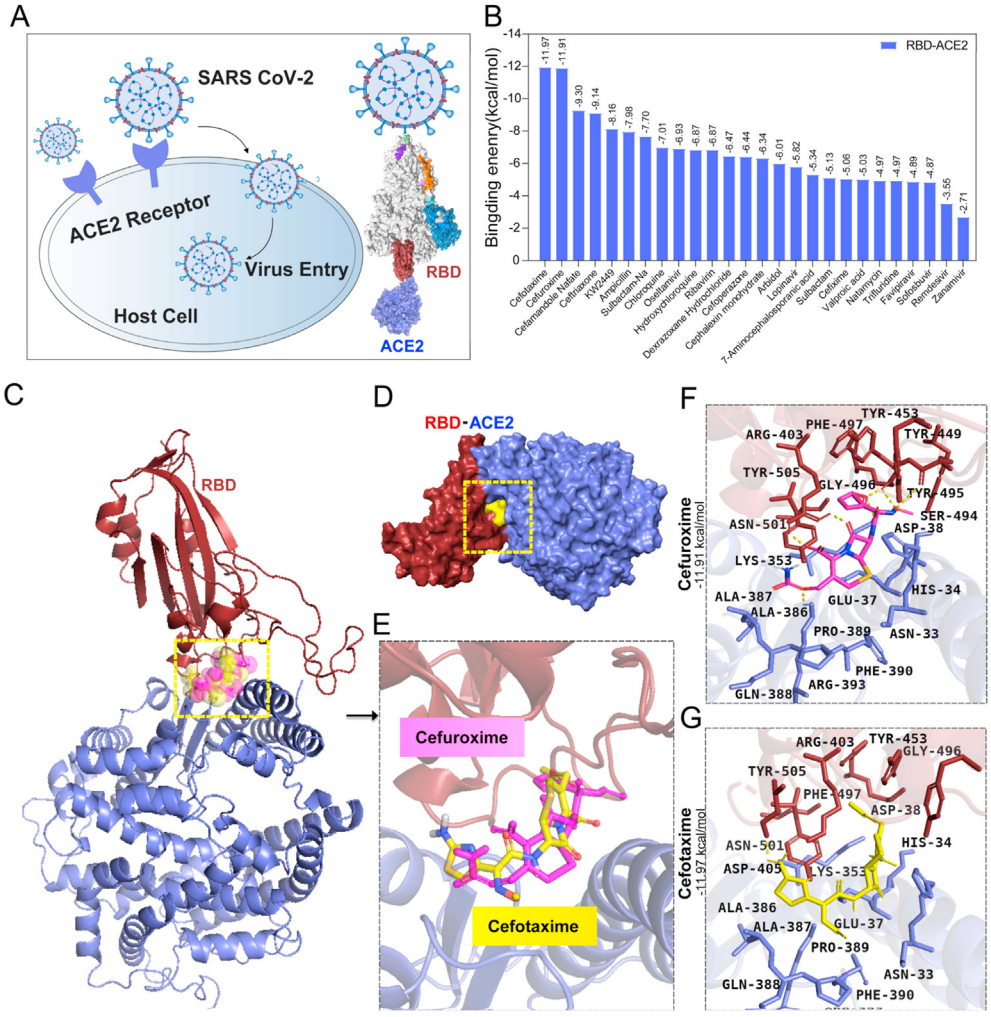

Figure 6. Screened drug-binding modes for RBD-ACE2 complex interaction. (A) Schematic illustration of the viral entry mechanism of SARS-CoV-2 to host cell through ACE2 receptor (*left*) and structure representation of S-RBD interaction with ACE2 (*right*). (B) Bar plot of binding affinities of screened candidates from chip and virtual screening and some representative FDA-approved antiviral drugs to RBD-ACE2 complex. (C and D) Cefuroxime and cefotaxime binding to RBD-ACE2 complex. The yellow dotted box indicates the binding area/pocket. (E) Close-up view of cefuroxime (magenta sticks) and cefotaxime (yellow sticks) binding to the RBD-ACE2 complex. (F and G) Close-up view of cefuroxime and cefotaxime binding mode and binding sites to the RBD-ACE2 complexes. Yellow dotted lines indicate H-bond.

structure of RBD-ACE2 (PDB ID: 6M0J) is employed in this ensemble docking.

As shown in Figure 6C, the ensemble docking on RBD-ACE2 receptors suggests that both cefuroxime and cefotaxime have excellent binding affinities toward the RBD-ACE2 complex (cefuroxime: -11.91 kcal/mol, cefotaxime: -11.97 kcal/mol). The data in Figure 6D-G shows that the drugs interact with RBD-ACE2 complex in the interface region of S-RBD (Arg^{403}, Tyr^{453}, Trp^{495}, Gly^{496}, Phe^{497}, $Asn^{501}$and Tyr^{505}) and ACE2 (Asn^{33}, His^{34}, Glu^{37}, Asp^{38}, Lys^{353}, Ala^{386}, Ala^{387}, Gln^{388}, Pro^{389}, Phe^{390} and Arg^{393}). Within these residues, Tyr^{453}, Gly^{496}, Asn^{501} and Tyr^{505} in S-RBD and His^{34}, Glu^{37}, Asp^{38} and Lys^{353} of ACE2 are reported to be the direct interface sites for S-RBD and ACE2 interaction [10], proving that cefuroxime and cefotaxime would affect the RBD-ACE2 complex via occupying the interface.

Besides, the complex structure of SARS-CoV-2 trimer spike glycoprotein and its receptor ACE2 revealed by cryo-EM shows that residue Tyr^{505} of SARS-CoV-2 RBD is the key amino acid required for ACE2 receptor binding [36], which is capable to eliminate the binding of ACE2. As shown in Figure 6F-G, Tyr^{505} also is involved in the binding between cefuroxime/cefotaxime and RBD-ACE2. The data indicate that cefuroxime and cefotaxime could affect the attachment of S-RBD to its ACE2 receptor in the host cell by blocking Tyr^{505}.

Furthermore, cefuroxime and cefotaxime also have slightly different binding modes towards the RBD-ACE2 complex. The presence of cefuroxime generates conventional hydrogen bonds with Lys^{353} and Arg^{393} in ACE2 and Gly^{496} and Arg^{403} in S-RBD, along with hydrophobic interactions, π–π stacking and carbon-hydrogen bonds with His^{34}, Glu^{37}, Ala^{387}, Arg^{393}, Lys^{353} in ACE2 and Tyr^{495}, Arg^{403} and Tyr^{505} in S-RBD (Figure 6F and S6A-C).

As for cefotaxime, conventional hydrogen bonds are formed with Arg^{393}, Glu^{37}, His^{34}, Lys^{353} in ACE2 subunit, and Arg^{403}, Asp^{405}, Gly^{496} in the S-RBD domain. Some other amino acids like His^{34}, Lys^{353} in ACE2 subunit and Tyr^{505}, Trp^{495} from S-RBD forms hydrophobic interactions and carbon-hydrogen bonds with the molecule (Figure 6G and S6D-F). The differences between cefuroxime and cefotaxime seem to be due to the variation of its chemical structures.

3. Conclusion

Given the limitation of new therapeutic agents' development for SARS-CoV-2 infections and its urgent clinical need, quick identification and re-purposing of active anti-viral molecules from the approved clinical usage drugs would be a viable strategy. Combining chip screening and virtual docking approach, this project provides a detailed study of the candidate inhibitors in the vital structural domains of the SARS-CoV-2 virus, including N-NTD, N-CTD, and S-RBD. 3142 small molecule candidates are evaluated via compounds library chip platform. Molecular docking shows the detailed information of these drugs with target proteins in the binding forms and binding sites. Two cephalosporin antibiotics, ceftriaxone and cefuroxime, are found to be the best among all the molecules. Moreover, cefuroxime and cefotaxime seem to occupy the interaction interface of S-RBD and ACE2 complex, leading to the interruption of host recognition. Arg^{403}, Tyr^{453}, Trp^{495}, Gly^{496}, Phe^{497}, $Asn^{501}$and Tyr^{505} in S-RBD and Asn^{33}, His^{34}, Glu^{37}, Asp^{38}, Lys^{353}, Ala^{386}, Ala^{387}, Gln^{388}, Pro^{389}, Phe^{390} and Arg^{393} in ACE2 are identified to be the critical interface sites. Besides, cefuroxime and cefotaxime are found to have an influence on the residue Tyr^{505} of SARS-CoV-2 RBD, which is the key amino acid required for ACE2 receptor binding. Overall, the output from this study could be extended for the screens of drugs against the novel virus breakout along with possible guidance for pharmacologists in future antiviral drug development.

In our subsequent studies, we plan to conduct in *vitro* and in *vivo* evaluation of the drug candidates obtained, as well as preparation for clinical trial application. Although a great deal of research has been carried out to identify effective inhibitors [37], it is necessary to have a variety of efficient treatment regimens for SARS-CoV-2, in order to maximize therapeutic efficacy and minimize the development of viral resistance. Overall, the project provides a novel, feasible strategy for therapeutic screening within existing cost limits, which could further reduce the pre-clinical trial time and help combat the SARS-CoV-2 pandemic.

4. Methods

4.1. Protein labeling and detection

The proteins were purchased from Hangzhou Ebiocore Biotechnology Co., Ltd. The protein concentration was determined by BCA methods, the purity and molecular weight are detected by SDS-PAGE. The protein was labeled with Cy5 using a CyDye Protein Labeling Cy5™ Mono-Reactive Dye Pack [26] (GE Healthcare, Little Chalfont, UK). The efficiency of labeling was verified by regular Dot Blot on a nitrocellulose membrane strip Dot blot [38].

4.2. Compounds database and chip incubation

The small molecule database contained 3,142 known molecules including FDA-approved clinical drugs, chemicals isolated from traditional Chinese herbals, and commercially available compounds (Figure 1G). The compounds were printed into the chip according to the literature [19, 20]. The printed microarray was commercially produced from Guangzhou Bochong Biological Technology Co., Ltd.

The incubation method is conducted according to literature with some modification [19, 23, 24]. Briefly, the printed microarray (stored at -80 °C) was immersed in blocking solution (3 mL 10% BSA with 7 mL PBS); the mixture was shaken by a side-swing shaker for an hour at room conditions; ultrapure water was then used to clean the chip; after drying in a chip dryer, the chip was scanned at 635 nm by using the chip fluorescence scanner (CapitalBio,=http://www.capitalbiotech.com/about.html?categoryId=28 Luxscan TM 10K-A). After the collection of the background signals, the printed microarray was cleaned with ultrapure water and then immersed in blocking solution (3 mL 10% BSA, 7 mL 1×PBS); the chip was then placed face up in the well of a 4-well rectangular Petri dish; 3 mL of Cy5 labeled protein solution was gently added into the slide bar code sticker and diffused over the chip; lidded the plate and placed the mixture on a shaking platform, allowing the solution to stir gently over the surface of the slide; after incubation with protein, the chip was cleaned in PBST (Phosphate Buffered Saline with 0.05% Tween 20) three times (5 min/time) at room conditions, following by ultrapure water (2 times 5 min/time); the cleaned chip was then centrifuged to dry and scanned at 635 nm by using the chip fluorescence scanner (CapitalBio,=http://www.capitalbiotech.com/about.html?categoryId=28 Luxscan TM 10K-A). All the procedures were processed under dark.

4.3. Data processing

Fluorescence intensity of small molecule chip was extracted from the microarray images by GenePix Pro 6.0 (Molecular Devices, Sunnyvale, CA). For molecules screening, the signal to noise ratio (SNR) is defined as the ratio of the median of the foreground signal to the median of the background signal [39]. The SNR of each protein was averaged for the triplicated spots on the microarray. Proteins with positive signals were identified on the array based on the assumption that SNR values across the array followed a normal distribution. SNR values were assigned to each protein by calculating (i.e., the distance from the mean of the reference SNR distribution, in units of SD). Cutoff = (meanSNR635 + 1.96×SD SNR635) (95%CI). SNR ≥ cutoff is set to call candidate N-interacting/S-RBD interacting small molecules. Proteins with SNR ≥ cutoff were considered to potentially positive small molecules. Fold change was set to SNR635 (first scan)/SNR635 (second scan). Proteins with fold change (FC) ≥ 1.2 were considered to effectively bind positive small molecules.

4.4. Protein preparation

The three-dimensional structures of SARS-CoV-2 S-RBD protein (PDB ID: 7BWJ), N -NTD (PDB ID: 6WZQ), N-CTD (PDB ID: 6VYO) were taken from the RCSB Protein Data Bank (PDB) (http://www.rcsb.org/), a worldwide archive resource of the crystal structure of biological macromolecules [40]. The protein was processed by autodock software, including the distribution of bond order, adding hydrogen, removing all water molecules, and calculating the Gasteiger charge and incorporation of nonpolar hydrogen. Then, the *pdbqt* file format of the protein was obtained according to the standard program.

4.5. Ligand preparation

PubChem is a chemical substance and biological activity repository, composed of three databases, including substances, compounds, and bioassay databases, which provide useful comprehensive chemical information for drug discovery [41]. The ligand structures were taken from PubChem databases server in 2D or 3D *sdf* format (https://pubchem.ncbi.nlm.nih.gov/). Then the *sdf* files of 2D were converted to mol2 files using Chemdraw software. After that, all the *sdf* files of 3D and mol2 were converted to *pdb* files using Pymol software and carry out hydrogenation and water removal treatment. After optimization, these files were loaded into AutoDock software for the final preparation of ligands and the standard process was run to obtain the *pdbqt* file.

4.6. Molecular docking

The docking of SARS-CoV-2 S protein, N protein, and ACE2 with the 16 molecules was performed with the aid of AutoDock Tools. Table S1 shows that the domain N-NTD, N-CTD, and S-RBD of SARS-CoV-2 target protein were obtained from the Protein Data Bank (PDB). The binding affinities and the interaction of SARS-CoV-2 S protein and N protein with the target molecule were predicted and analyzed using the same software. The grid box center is designed to be at X: -12.576, Y: -11.504, Z: 25.512 (PDB:7BWJ), X: -14.508, Y: 11.082, Z: 18.105 (PDB:6WZQ), X: -13.209, Y: 19.051, Z: 9.014 (PDB:6VYO) with a suitable grid box volume where the ligands can easily be fitted. After calibration and optimization, we use the same mesh box size and other parameters for docking research and run the entire setup to get different docking conformations. In order to visualize and detect non-covalent interactions in docked drug-protein complexes, PyMol (version 3.7.2) and Discovery Studio Visualizer 2020 Client software were utilized for the docking analyses.

4.7. The calculation of binding energy

According to the previous research [42], the free energy (ΔG) of binding is calculated via the energy difference between the ligand & protein in the separated unbound state and the binding state. Two evaluation steps were included: first, separately assess the intramolecular energetics of the transition from the unbound state to the bound conformation of each molecule; Second, assess the intermolecular energetics of the combination of two molecules into a binding complex.

As shown in Eqs. (1) and (2), the free energy (ΔG) includes six pairs of evaluation (V) and estimation of conformational entropy lost after binding ($\Delta S_{conf} S_{conf}$).

$$\Delta G = V_{bound}^{L-L} - V_{unbound}^{L-L} + \left(V_{bound}^{P-P} - V_{unbound}^{P-P}\right) + \left(V_{bound}^{P-L} - V_{unbound}^{P-L} + \Delta S_{conf}\right) \quad (1)$$

$$\Delta S_{conf} = W_{conf} N_{tors} \quad (2)$$

where, L is ligand;

P is protein;

V_{bound}^{L-L} and $V_{unbound}^{L-L}$ are the intramolecular energies of bound and unbound states of the ligand;

V_{bound}^{P-P} and $V_{unbound}^{P-P}$ are the intramolecular energies of bound and unbound states of the protein;

V_{bound}^{P-L} and $V_{unbound}^{P-L}$ are the change of intermolecular energy between bound and unbound states, assuming $V_{unbound}^{P-L} = 0$, when the two molecules are sufficiently distant from one another in the unbound state;

W_{conf} is weighting constants;

N_{tors} is rotatable bonds in the molecule, which include all torsional degrees of freedom, such as rotation of polar hydrogen atoms on hydroxyl groups and the like.

4.8. Toxicity evaluation of compounds in vero cells

Vero cells were seeded to a 96-well plate with 1×10^4 cells/well and incubated at 37 °C incubator overnight, supplement with 5% CO_2. The small molecule drugs were diluted gradually from 20 μM in half to 0.3125 μM, with 7 concentration gradients and three replicates per gradient. Then the culture medium was sucked and discarded, the diluted drug was added, and the culture was continued at 37 °C for 48 h. After 48 h of incubation, a colorimetric assay for the determination of cell viability (Cell counting kit-8; CCK-8) was performed. The CCK8 solution (10 μL) was added to each well and incubated for 2 h. The absorbance of the solution was measured at 450 nm (Epoch 2, BioTek Instruments, Inc., USA). The half-maximal inhibitory concentration (IC_{50}) values were calculated using the PrismPad program (Version5.0, GraphPad Software, San Diego, CA, USA). The Prism 9 software was used to plot the curves.

Declarations

Author contribution statement

Xuqiao Hu: Conceived and designed the experiments; Performed the experiments; Analyzed and interpreted the data; Wrote the paper.

Zhenru Zhou: Performed the experiments; Analyzed and interpreted the data.

Fei Li; Yang Xiao; Zhaoyang Wang: Performed the experiments.

Jinfeng Xu; Fajin Dong; Hairong Zheng; Rongmin Yu: Contributed reagents, materials, analysis tools or data; Wrote the paper.

Funding statement

This work was supported by the Commission of Scientific and Technology of Shenzhen (grant no. JCYJ20190806151807192).

Data availability statement

Data will be made available on request.

Declaration of interests statement

The authors declare no conflict of interest.

Additional information

Supplementary content related to this article has been published online at https://doi.org/10.1016/j.heliyon.2021.e06387.

Acknowledgements

We thank Ebiocore Biotechnology Co., Ltd. for the providing of pure proteins, thanks for Discovery Studio Visualizer 2020 software provider. We thank Dr. Dongbo Yu from The University of Chicago for the advice on the antiviral drugs in clinical practice and editing of the manuscript.

References

[1] C. Huang, Y. Wang, X. Li, L. Ren, J. Zhao, Y. Hu, L. Zhang, G. Fan, J. Xu, X. Gu, Z. Cheng, T. Yu, J. Xia, Y. Wei, W. Wu, X. Xie, W. Yin, H. Li, M. Liu, Y. Xiao, H. Gao, L. Guo, J. Xie, G. Wang, R. Jiang, Z. Gao, Q. Jin, J. Wang, B. Cao, Clinical features of patients infected with 2019 novel coronavirus in Wuhan, China, Lancet 395 (2020) 497–506.

[2] J.F.W. Chan, S. Yuan, K.H. Kok, K.K.W. To, H. Chu, J. Yang, F. Xing, J. Liu, C.C.Y. Yip, R.W.S. Poon, H.W. Tsoi, S.K.F. Lo, K.H. Chan, V.K.M. Poon, W.M. Chan, J.D. Ip, J.P. Cai, V.C.C. Cheng, H. Chen, C.K.M. Hui, K.Y. Yuen, A familial cluster of pneumonia associated with the 2019 novel coronavirus indicating person-to-person transmission: a study of a family cluster, Lancet 395 (2020) 514–523.

[3] H.W. Jiang, Y. Li, H.N. Zhang, W. Wang, X. Yang, H. Qi, H. Li, D. Men, J. Zhou, S.C. Tao, SARS-CoV-2 proteome microarray for global profiling of COVID-19 specific IgG and IgM responses, Nat. Commun. 11 (2020) 3581.

[4] P. Zhou, X.L. Yang, X.G. Wang, B. Hu, L. Zhang, W. Zhang, H.R. Si, Y. Zhu, B. Li, C.L. Huang, H.D. Chen, J. Chen, Y. Luo, H. Guo, R.D. Jiang, M.Q. Liu, Y. Chen, X.R. Shen, X. Wang, X.S. Zheng, K. Zhao, Q.J. Chen, F. Deng, L.L. Liu, B. Yan, F.X. Zhan, Y.Y. Wang, G.F. Xiao, Z.L. Shi, A pneumonia outbreak associated with a new coronavirus of probable bat origin, Nature 579 (2020) 270–273.

[5] P.C.Y. Woo, Y. Huang, S.K.P. Lau, K.-Y. Yuen, Coronavirus Genomics and Bioinformatics Analysis, Viruses 2, 2010, pp. 1804–1820.

[6] P.K. Panda, M.N. Arul, P. Patel, S.K. Verma, W. Luo, H.G. Rubahn, Y.K. Mishra, M. Suar, R. Ahuja, Structure-based drug designing and immunoinformatics approach for SARS-CoV-2, Sci. Adv. 6 (2020), eabb8097.

[7] F. Li, W. Li, M. Farzan, S.C. Harrison, Structure of SARS coronavirus spike receptor-binding domain complexed with receptor, Science 309 (2005) 1864–1868.

[8] D. Wrapp, N.S. Wang, K.S. Corbett, J.A. Goldsmith, C.L. Hsieh, O. Abiona, B.S. Graham, J.S. McLellan, Cryo-EM structure of the 2019-nCoV spike in the prefusion conformation, Science 367 (2020) 1260–1263.

[9] Y. Cong, M. Ulasli, H. Schepers, M. Mauthe, P. V'Kovski, F. Kriegenburg, V. Thiel, C.A.M. de Haan, F. Reggiori, Nucleocapsid protein recruitment to replication-transcription complexes plays a crucial role in coronaviral life cycle, J. Virol. 94 (2020), e01925, 19.

[10] J. Lan, J.W. Ge, J.F. Yu, S.S. Shan, H. Zhou, S.L. Fan, Q. Zhang, X.L. Shi, Q.S. Wang, L.Q. Zhang, X.Q. Wang, Structure of the SARS-CoV-2 spike receptor-binding domain bound to the ACE2 receptor, Nature 581 (2020) 215–220.

[11] L. Malle, A map of SARS-CoV-2 and host cell interactions, Nat. Rev. Immunol. 20 (2020) 351.

[12] A.C. Walls, Y.J. Park, M.A. Tortorici, A. Wall, A.T. McGuire, D. Veesler, Structure, function, and antigenicity of the SARS-CoV-2 spike glycoprotein, Cell 183 (2020) 1735.

[13] S. Kang, M. Yang, Z. Hong, L. Zhang, Z. Huang, X. Chen, S. He, Z. Zhou, Z. Zhou, Q. Chen, Y. Yan, C. Zhang, H. Shan, S. Chen, Crystal structure of SARS-CoV-2 nucleocapsid protein RNA binding domain reveals potential unique drug targeting sites, Acta Pharm. Sin. B. 10 (2020) 1228–1238.

[14] Q. Ye, A.M.V. West, S. Silletti, K.D. Corbett, Architecture and self-assembly of the SARS-CoV-2 nucleocapsid protein, Protein Sci. (2020) 1890–1901.

[15] M. Wang, R. Cao, L. Zhang, X. Yang, J. Liu, M. Xu, Z. Shi, Z. Hu, W. Zhong, G. Xiao, Remdesivir and chloroquine effectively inhibit the recently emerged novel coronavirus (2019-nCoV) in vitro, Cell Res. 30 (2020) 269–271.

[16] B. Cao, Y. Wang, D. Wen, W. Liu, J. Wang, G. Fan, L. Ruan, B. Song, Y. Cai, M. Wei, X. Li, J. Xia, N. Chen, J. Xiang, T. Yu, T. Bai, X. Xie, L. Zhang, C. Li, Y. Yuan, H. Chen, H. Li, H. Huang, S. Tu, F. Gong, Y. Liu, Y. Wei, C. Dong, F. Zhou, X. Gu, J. Xu, Z. Liu, Y. Zhang, H. Li, L. Shang, K. Wang, K. Li, X. Zhou, X. Dong, Z. Qu, S. Lu, X. Hu, S. Ruan, S. Luo, J. Wu, L. Peng, F. Cheng, L. Pan, J. Zou, C. Jia, J. Wang, X. Liu, S. Wang, X. Wu, Q. Ge, J. He, H. Zhan, F. Qiu, L. Guo, C. Huang, T. Jaki, F.G. Hayden, P.W. Horby, D. Zhang, C. Wang, A trial of lopinavir-ritonavir in adults hospitalized with severe covid-19, N. Engl. J. Med. 382 (2020) 1787–1799.

[17] D.R. Calabrese, K. Zlotkowski, S. Alden, W.M. Hewitt, C.M. Connelly, R.M. Wilson, S. Gaikwad, L. Chen, R. Guha, C.J. Thomas, B.A. Mock, J.S. Schneekloth, Characterization of clinically used oral antiseptics as quadruplex-binding ligands, Nucleic Acids Res. 46 (2018) 2722–2732.

[18] N.B. Struntz, A. Chen, A. Deutzmann, R.M. Wilson, E. Stefan, H.L. Evans, M.A. Ramirez, T. Liang, F. Caballero, M.H.E. Wildschut, D.V. Neel, D.B. Freeman, M.S. Pop, M. McConkey, S. Muller, B.H. Curtin, H. Tseng, K.R. Frombach, V.L. Butty, S.S. Levine, C. Feau, S. Elmiligy, J.A. Hong, T.A. Lewis, A. Vetere, P.A. Clemons, S.E. Malstrom, B.L. Ebert, C.Y. Lin, D.W. Felsher, A.N. Koehler, Stabilization of the max homodimer with a small molecule attenuates myc-driven transcription, Cell Chem. Biol. 26 (2019) 711–723.

[19] Z. Li, C. Wang, Z. Wang, C. Zhu, J. Li, T. Sha, L. Ma, C. Gao, Y. Yang, Y. Sun, J. Wang, X. Sun, C. Lu, M. Difiglia, Y. Mei, C. Ding, S. Luo, Y. Dang, Y. Ding, Y. Fei, B. Lu, Allele-selective lowering of mutant HTT protein by HTT-LC3 linker compounds, Nature 575 (2019) 203–209.

[20] C.M. Connelly, F.A. Abulwerdi, J.S. Schneekloth, Discovery of RNA binding small molecules using small molecule microarrays, Methods Mol. Bol. 1518 (2017) 157–175.

[21] F.A. Abulwerdi, W. Xu, A.A. Ageeli, M.J. Yonkunas, G. Arun, H. Nam, J.S. Schneekloth Jr., T.K. Dayie, D. Spector, N. Baird, S.F.J. Le Grice, Selective small-molecule targeting of a triple helix encoded by the long noncoding RNA, MALAT1, ACS Chem. Biol. 14 (2019) 223–235.

[22] S.N. Journey, S.L. Alden, W.M. Hewitt, M.L. Peach, M.C. Nicklaus, J.S. Schneekloth Jr., Probing the hras-1(Y) i-motif with small molecules, Medchemcomm 9 (2018) 2000–2007.

[23] J.E. Bradner, O.M. McPherson, A.N. Koehler, A method for the covalent capture and screening of diverse small molecules in a microarray format, Nat. Protoc. 1 (2006) 2344–2352.

[24] C. Zhu, X. Zhu, J.P. Landry, Z. Cui, Q. Li, Y. Dang, L. Mi, F. Zheng, Y. Fei, Developing an efficient and general strategy for immobilization of small molecules onto microarrays using isocyanate chemistry, Sensors 16 (2016) 378.

[25] J.M. Kim, B.L. Seong, Highly chromophoric Cy5-methionine for N-terminal fluorescent tagging of proteins in eukaryotic translation systems, Sci. Rep. 7 (2017) 11642.

[26] C.J. Hu, J.B. Pan, G. Song, X.T. Wen, Z.Y. Wu, S. Chen, W.X. Mo, F.C. Zhang, J. Qian, H. Zhu, Y.Z. Li, Identification of novel biomarkers for behcet disease diagnosis using human proteome microarray approach, Mol. Cell. Proteomics 16 (2017) 147–156.

[27] J. Sztuba-Solinska, S.R. Shenoy, P. Gareiss, L.R. Krumpe, S.F. Le Grice, B.R. O'Keefe, J.S. Schneekloth Jr., Identification of biologically active, HIV TAR RNA-binding small molecules using small molecule microarrays, J. Am. Chem. Soc. 136 (2014) 8402–8410.

[28] C.P. Dooley, A.W. Larson, N.H. Stace, et al., Double-contrast barium meal and upper gastrointestinal endoscopy: a comparative study, Ann. Intern. Med. 101 (1984) 538–545.

[29] F. Cafini, L. Aguilar, L. Alou, M.J. Gimenez, D. Sevillano, M. Torrico, N. Gonzalez, J.J. Granizo, J.E. Martin-Herrero, J. Prieto, Cidal activity of oral third-generation cephalosporins against Streptococcus pneumoniae in relation to cefotaxime intrinsic activity, Eur. J. Clin. Microbiol. Infect. Dis. 27 (2008) 679–683.

[30] C.-H. Tai, M. Bellesi, A.-C. Chen, C.-L. Lin, H.-H. Li, P.-J. Lin, W.-C. Liao, C.-S. Hung, R.K. Schwarting, Y.-J. Ho, A new avenue for treating neuronal diseases: ceftriaxone, an old antibiotic demonstrating behavioral neuronal effects, Behav. Brain Res. 364 (2019) 149–156.

[31] S. Lu, Q. Ye, D. Singh, Y. Cao, J.K. Diedrich, J.R. Yates 3rd, E. Villa, D.W. Cleveland, K.D. Corbett, The SARS-CoV-2 nucleocapsid phosphoprotein forms mutually exclusive condensates with RNA and the membrane-associated M protein, Nat. Commun. 12 (2021) 502.

[32] C.K. Chang, C.M. Chen, M.H. Chiang, Y.L. Hsu, T.H. Huang, Transient oligomerization of the SARS-CoV N protein-implication for virus ribonucleoprotein packaging, PloS One 8 (2013), e65045.

[33] C.K. Chang, S.C. Sue, T.H. Yu, C.M. Hsieh, C.K. Tsai, Y.C. Chiang, S.J. Lee, H.H. Hsiao, W.J. Wu, W.L. Chang, C.H. Lin, T.H. Huang, Modular organization of SARS coronavirus nucleocapsid protein, J. Biomed. Sci. 13 (2006) 59–72.

[34] L.M. Lima, B. Silva, G. Barbosa, E.J. Barreiro, beta-lactam antibiotics: an overview from a medicinal chemistry perspective, Eur. J. Med. Chem. 208 (2020) 112829.

[35] C. Wu, Y. Liu, Y. Yang, P. Zhang, W. Zhong, Y. Wang, Q. Wang, Y. Xu, M. Li, X. Li, M. Zheng, L. Chen, H. Li, Analysis of therapeutic targets for SARS-CoV-2 and discovery of potential drugs by computational methods, Acta Pharm. Sin. B (2020) 766–788.

[36] C. Xu, Y. Wang, C. Liu, C. Zhang, W. Han, X. Hong, Y. Wang, Q. Hong, S. Wang, Q. Zhao, Y. Wang, Y. Yang, K. Chen, W. Zheng, L. Kong, F. Wang, Q. Zuo, Z. Huang, Y. Cong, Conformational dynamics of SARS-CoV-2 trimeric spike glycoprotein in complex with receptor ACE2 revealed by cryo-EM, Sci. Adv. 7 (2020) eabe5575.

[37] R. Wu, L. Wang, H.D. Kuo, A. Shannar, R. Peter, P.J. Chou, S. Li, R. Hudlikar, X. Liu, Z. Liu, G.J. Poiani, L. Amorosa, L. Brunetti, A.N. Kong, An update on current therapeutic drugs treating COVID-19, Curr. Pharmacol. Rep. (2020) 1–15.

[38] J.G. Costa, M.J. Vilarino, Semiquantitative Dot Blot with the GRA8 antigen to differentiate the stages of toxoplasmosis infection, J. Microbiol. Methods 149 (2018) 9–13.

[39] A.M. Sadaghiani, S.M. Lee, J.I. Odegaard, D.B. Leveson-Gower, O.M. McPherson, P. Novick, M.R. Kim, A.N. Koehler, R. Negrin, R.E. Dolmetsch, C.Y. Park, Identification of Orai1 channel inhibitors by using minimal functional domains to screen small molecule microarrays, Chem. Biol. 21 (2014) 1278–1292.

[40] S.K. Burley, H.M. Berman, C. Christie, J.M. Duarte, Z. Feng, J. Westbrook, J. Young, C. Zardecki, RCSB Protein Data Bank: sustaining a living digital data resource that enables breakthroughs in scientific research and biomedical education, Protein Sci. 27 (2018) 316–330.

[41] S. Kim, Getting the most out of PubChem for virtual screening, Expet Opin. Drug Discov. 11 (2016) 843–855.

[42] R. Huey, G.M. Morris, A.J. Olson, D.S. Goodsell, A semiempirical free energy force field with charge-based desolvation, J. Comput. Chem. 28 (2007) 1145–1152.